The International Journal of Advanced Manufacturing Technology (2024) 133:2533–2550
https://doi.org/10.1007/s00170-024-13939-4

ORIGINAL ARTICLE

# Simulation and experimental study on microgrinding mechanism and machining morphology of ITO conductive glass

Xingwei Sun[1,2] · Xiaolong Qiu[1,2] · Yin Liu[1,2] · Fei Pan[1,2] · Jiahao Chen[1,2] · Weifeng Zhang[1,2] · Zhixu Dong[1,2] · Heran Yang[1,2]

Received: 1 January 2024 / Accepted: 27 May 2024 / Published online: 10 June 2024
© The Author(s), under exclusive licence to Springer-Verlag London Ltd., part of Springer Nature 2024

**Abstract**
The analysis of the grinding mechanism of ITO conductive glass is particularly important for revealing material damage and chip formation. This article proposes the removal mechanism of brittle thin film materials during grinding based on the indentation model. And based on the thin film composite structure of ITO conductive glass, a material model in finite element simulation was established. The surface morphology and chip state of ITO conductive glass were studied through microscale grinding experiments. By comparing the simulation results, it has been proven that the ITO film is removed in a brittle fracture mode during the grinding process, while the removal mode of the glass substrate is influenced by the process parameters. The interlayer fracture between the film and substrate will affect the processing quality.

**Keywords** ITO conductive glass · Finite element simulation · Grinding mechanism · Machining morphology

## 1 Introduction

ITO conductive glass can be obtained by sputtering a layer of ITO film on soda-lime glass and annealing at high temperature. Because of its high hardness, corrosion resistance, high infrared reflectance, and high microwave attenuation, it is widely used in aircraft defogging windows, building glass curtain walls, radar shielding, and other aspects [1]. ITO thin films deposited on glass substrates by magnetron sputtering are amorphous. After heat treatment, crystalline ITO thin films composed of cubic $In_2O_3$ cells can be obtained. At this time, ITO conductive glass is a thin film composite material of brittle thin films and brittle substrates. However, there are differences in mechanical properties between the film layer and the substrate material, which will cause stress and strain mismatch during the processing of the film composite and affect the function of the film substrate system.

In order to evaluate the material properties and establish the material constitutive model, it is necessary to obtain the mechanical property parameters of the film material. The free film test method is the most direct and accurate method for mechanical characterization of thin film materials. Oh et al. [2] used femtosecond laser technology to produce substrate free ITO films and conducted tensile tests on individual ITO films to obtain the elastic modulus and tensile strength of ITO films at different annealing temperatures. However, the preparation cost of free film is high, and the film thickness is small, so it is not easy to clamp. Qu et al. [3] conducted nanoindentation experiments on oxide films on SiC substrates and proposed a characterization method of film indentation mechanical properties considering substrate effects. Wang et al. [4] compared single-layer ITO film and multi-layer film on glass substrate, analyzed the relationship between film mechanical properties and film morphology through indentation test, and concluded that heat treatment method affected the ratio of hardness and elastic modulus, thus affecting the wear resistance of the film. Hengst et al. [5]

✉ Yin Liu
liuyin_neu@163.com

1 School of Mechanical Engineering, Shenyang University of Technology, Shenyang Economic and Technological Development District, NO.111, Shenliao West Road, Shenyang 110870, P.R. China

2 Liaoning Province Key Laboratory of Complex Surface NC Manufacturing Technology, Shenyang University of Technology, Shenyang Economic and Technological Development District, NO.111, Shenliao West Road, Shenyang 110870, P.R. China

studied the effect of ITO film microstructure on material morphology, Young's modulus, and crack initiation strain. The Young's modulus decreased with the increase of temperature, while the internal pressure generated by magnetron sputtering led to the increase of crack initiation strain with the increase of film thickness. Feng et al. [6] used Hopkins pressure bar to study the dynamic damage and fracture mode of ITO conductive glass, revealing the nucleation mechanism of crack and the influencing factors of fracture strength.

Grinding is the main method for efficient machining of brittle materials. Zhu et al. [7] used a single abrasive grain to study the crack evolution in SiC grinding process, and through experiments, it was proved that the material in the brittle region can be removed by lateral cracks, while increasing the wheel speed can suppress median cracks. Lin et al. [8] studied the surface and subsurface integrity during the grinding process of BK7 glass and concluded that the normal grinding force had the greatest impact on the surface roughness and subsurface damage during the grinding process of diamond wheel. Ma et al. [9] studied the fracture and removal mechanism of glass ceramics during grinding, and proposed an evaluation index of grinding quality based on the unchanged chip thickness theory to effectively judge the removal state of materials. Zhang et al. [10] used microstructure grinding wheel to grind zirconia, defined the critical grinding depth of three cutting states according to the grinding force, and verified the grinding force prediction model. Yang et al. [11] proposed a material flow stress field model for glass ceramics during ductile processing, and applied the brittle material removal mechanism at the microscale through the nanoscratch experiment. Sun et al. [12] used a new type of microgrinding tool to process sapphire, established a microgrinding force model considering structural parameters, size effect and material removal mechanism, and proved that the grinding tool can effectively reduce the grinding force and improve the processing quality.

At present, although many scholars have made a lot of research on the removal mechanism of brittle materials, the research on thin film composites is relatively less. In this paper, according to the material structure characteristics of ITO conductive glass, a simulation model of cutting film composites with a single abrasive particle is established to study the removal state of film and substrate under the cutting action of abrasive particles. The mechanism of material removal is analyzed, and the critical cutting thickness model of thin film is proposed combined with the indentation model of thin film. The micro scale grinding experiment of ITO conductive glass was carried out, and the machining morphology was analyzed through the abrasive trajectory, which confirmed the removal mechanism of brittle film material obtained by simulation.

## 2 Microgrinding mechanism of ITO conductive glass

### 2.1 Critical cutting thickness of ITO conductive glass material

The material removal method during the grinding process can be analyzed by the critical cutting depth $h_c$ and the undeformed chip thickness $h_m$ [13, 14]. When $h_m$ is less than $h_c$, the material forms chips through the sliding friction of abrasive particles and plowing in the plastic deformation zone, and the material is in a ductile removal mode. When the thickness of undeformed chips $h_m$ is greater than $h_c$, the material forms chips through the formation and propagation of cracks, and the material is in a ductile removal mode [15, 16]. It is currently widely believed that there exists a removal mode where both ductile and brittle characteristics coexist when $h_m$ approaches $h_c$, and the specific relationship is as follows [17]:

$$h_m = \begin{cases} h_m \le h_{c1} & \text{Ductile} \\ h_{c1} < h_m \le h_{c2} & \text{Brittle} - \text{ductile} \\ h_{c2} < h_m & \text{Brittle} \end{cases} \tag{1}$$

Microscale grinding can be seen as the collaborative cutting of microabrasive particles and microedges on the surface of a microgrinding wheel to form the surface material for machining parts. The use of indentation fracture model, treating the indenter as a simplified model of abrasive particles, can effectively analyze the crack propagation and material removal mechanism of brittle materials during the grinding process 18.

The block material indentation model is shown in. Fig. 1 a, and the relationship between the load $P$ of the indenter and the indentation size $2a$ is [19]:

$$P = \xi H_v a^2 \tag{2}$$

where ξ is the geometric coefficient of the workpiece material and $\xi = 2\times H_v$; $H_v$ is the hardness of the workpiece material.

According to the indentation test of brittle materials, when the applied load is less than the critical load, the material only undergoes plastic deformation. When the load exceeds the critical load, the material will undergo brittle fracture. Among them, the critical load can be expressed as follows:

$$P^* = 54.5\left(\frac{a}{\eta^2\gamma^2}\right)\frac{K_{IC}^4}{H_v^3} \tag{3}$$

where $\alpha$, $\eta$, and $\gamma$ is a dimensionless constant, for the indenter, $a = 2/\pi$, $\eta \approx 1$, $\gamma = 0.2K_{IC}$; $K_{IC}$ is the fracture toughness of the material.

As shown in Fig. 1a, the indentation feature size is $a = h\ \tan\theta$, $\theta$ is indenter characteristic half angle. So the

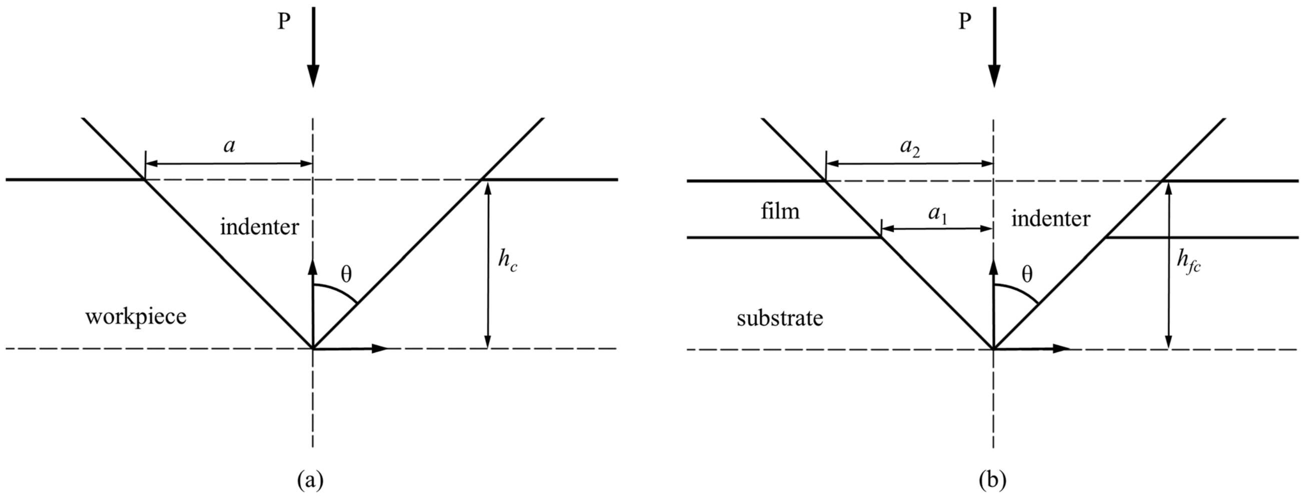


**Fig. 1** Indentation model. (**a**) Block material indentation principle diagram (**b**) Principle diagram of thin film material indentation

relationship between the indentation load $P$ and the depth of penetration $h$ is as follows:

$$P = k\xi \tan^2 \theta H_v h^2 \tag{4}$$

where $k$ is the percentage of the load head area to the indenter area, $0 \le k \le 1$.

When the indentation load $P$ is equal to the critical load $P^*$, the critical cutting depth $h_c$ of a single abrasive grain can be obtained [20]:

$$h_c = \left[ 54.5 \left( \frac{\alpha}{\eta^2 \gamma^2} \right) \frac{K_{IC}^4}{k\xi \tan^2 \theta H_v^4} \right]^{\frac{1}{2}} \tag{5}$$

As shown in Fig. 1b, when the indenter acts on the thin film material, the relationship between the indentation load $P_f$ and the depth of indentation $h_f$ can be expressed as follows:

$$\begin{cases} P_f = E_{rs} h_f a_2 (1 - \Delta) + E_{rf} h_f a_2 \Delta \\ \Delta = \sqrt{1 - \left( \frac{a_1}{a_2} \right)^2} - \cosh^{-1} \left( \frac{a_2}{a_1} \right) / \left( \frac{a_2}{a_1} \right)^2 \end{cases} \tag{6}$$

where $E_{rs}$ and $E_{rf}$ are the nominal elastic moduli of the substrate and thin film, respectively; $a_1$ and $a_2$ are the characteristic dimensions of the indentation, $a_2 = h_{fc} \tan\theta$; $\Delta$ is he characteristic coefficient of thin film indentation, $\Delta$ related to factors such as indentation depth, film thickness, and indenter characteristic half angle.

By equating the thin film indentation load $P_f$ in formula (6) with the critical load $P^*$ in formula (3), the critical cutting thickness $h_{fc}$ of the thin film material can be obtained through further derivation:

$$h_{fc} = \left[ 54.5 \left( \frac{\alpha}{\eta^2 \gamma^2} \right) \frac{K_{IC}^4}{H_v^3 \left( E_{rs} - E_{rs}\Delta + E_{rf}\Delta \right) \tan \theta} \right]^{\frac{1}{2}} \tag{7}$$

The surface of ITO conductive glass has a brittle thin film, and the fracture toughness of soda-lime glass adjacent to this film area is affected by the bonding effect of the film. However, due to the fact that the thickness of ITO thin films is much smaller than the thickness that can be achieved by micro grinding, the impact on the critical cutting thickness of soda-lime glass is relatively small. When applied to thin film materials, further correction of two factors is needed $\tau_1$, $\tau_2$ two ductility stage coefficients

$$h_{fc1} = \tau_1 h_{fc} \tag{8}$$

$$h_{fc2} = \tau_2 h_{fc} \tag{9}$$

where $\tau_1$ and $\tau_2$ represents the ductility stage coefficients for the transition of two removal modes.

## 2.2 Undeformed chip thickness in microgrinding

For microscale grinding using microgrinding tools with a diameter less than 1 mm, the grinding principle is similar to the traditional grinding wheel model when using cylindrical side abrasive particles of the micro grinding tool to perform side grinding on the workpiece [21], as shown in Fig. 2. In microscale grinding, the maximum undeformed chip thickness $h_m$ can be regarded as the AC length, which can be calculated by triangulation of the workpiece displacement s between abrasive particles. Due to the fact that the maximum undeformed chip thickness $h_m$ is much

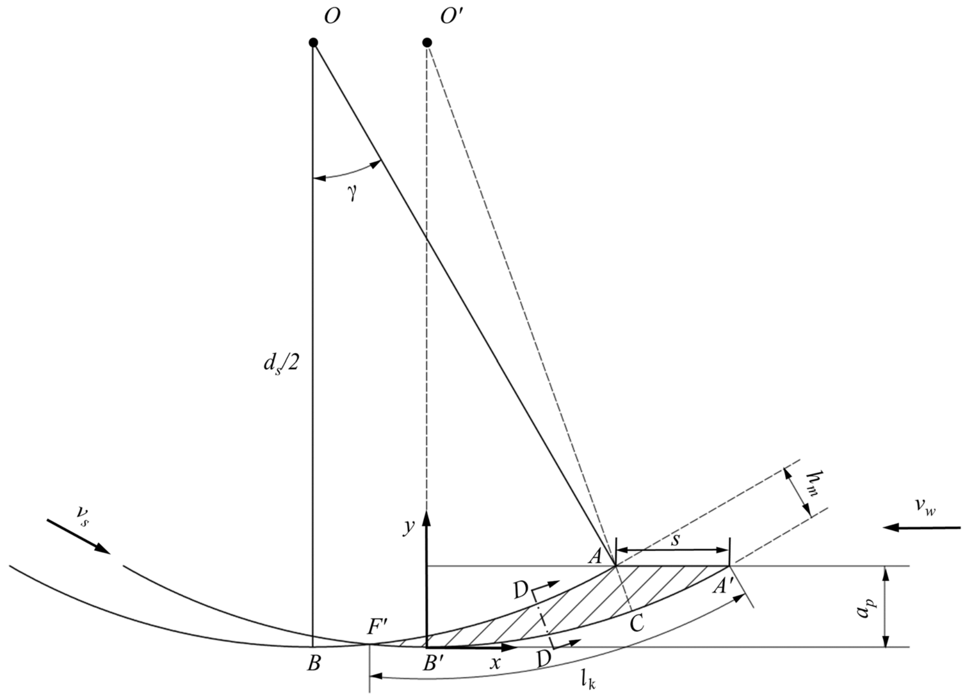


**Fig. 2** Geometric model of micro side grinding

smaller than the contact arc length $l_k$ of the abrasive particles, the undeformed chip thickness of microscale grinding in side grinding can be expressed as [17]:

$$h_m = 2M_d\left[\left(\frac{L_r v_w}{v_s}\right)\left(\frac{a_p}{d_s}\right)^{\frac{1}{2}}\left(1-\frac{a_p}{d_s}\right)^{\frac{1}{2}} - \frac{L_r{}^2}{d_s}\left(\frac{v_w}{v_s}\right)\right]^2 \tag{10}$$

where $M_d$ is the microscale grinding size effect coefficient, $L_r$ is the distance between abrasive particles, $v_w$ is the feed speed of the workpiece, and $v_s$ is the linear velocity of abrasive grain.

The schematic diagram of microscale grinding of ITO conductive glass is shown in Fig. 3a. The material of the workpiece is ITO conductive glass, with soda-lime glass as the substrate, and a thickness of about 0.2-μm ITO thin film is coated on the surface of the substrate. Using microgrinding tools with electroplated abrasive particles, microgrooves are machined on ITO conductive glass. In microscale groove grinding, the removal of material on the side of the microgroove can be considered as side grinding, but the grinding mechanism at the bottom of the microgroove is closer to vertical plane grinding. The schematic diagram of vertical plane grinding is shown in Fig. 3b. Under the conditions of high speed and low feed speed, it can be assumed that the main material removal is carried out by the abrasive grains on the outer side of the grinding tool. At this time, the undeformed chip thickness of vertical plane grinding is [22]:

$$\overline{h} = \frac{f}{nC_d\sqrt{1+\frac{B^2}{4d_s^2}}} \tag{11}$$

For the grinding of the bottom of the microgroove, the grinding width $B$ is the width of the microgroove, which is equal to the tool diameter $d_s$ of the microgrinding tool. By correcting the above formula, the average undeformed chip thickness of the bottom grinding of the microgroove grinding can be obtained as:

$$\overline{h} = \frac{2f}{\pi n C_d} \tag{12}$$

where $d_s$ is the diameter of the grinding tool, $B$ is the grinding width, $C_d$ is the circumferential abrasive particle density of the grinding tool, and $n$ is the rotating speed of the grinding tool.

Figure 4 shows the undeformed chip thickness of micro groove bottom grinding, where $g_a$ and $g_b$ represent two adjacent abrasive grains on the circumference of the grinding tool. As the grinding tool feeds, the shaded area enclosed by the trajectory of the two abrasive particles represents the cutting area of the abrasive particles. The maximum thickness of the shaded area is equal to the

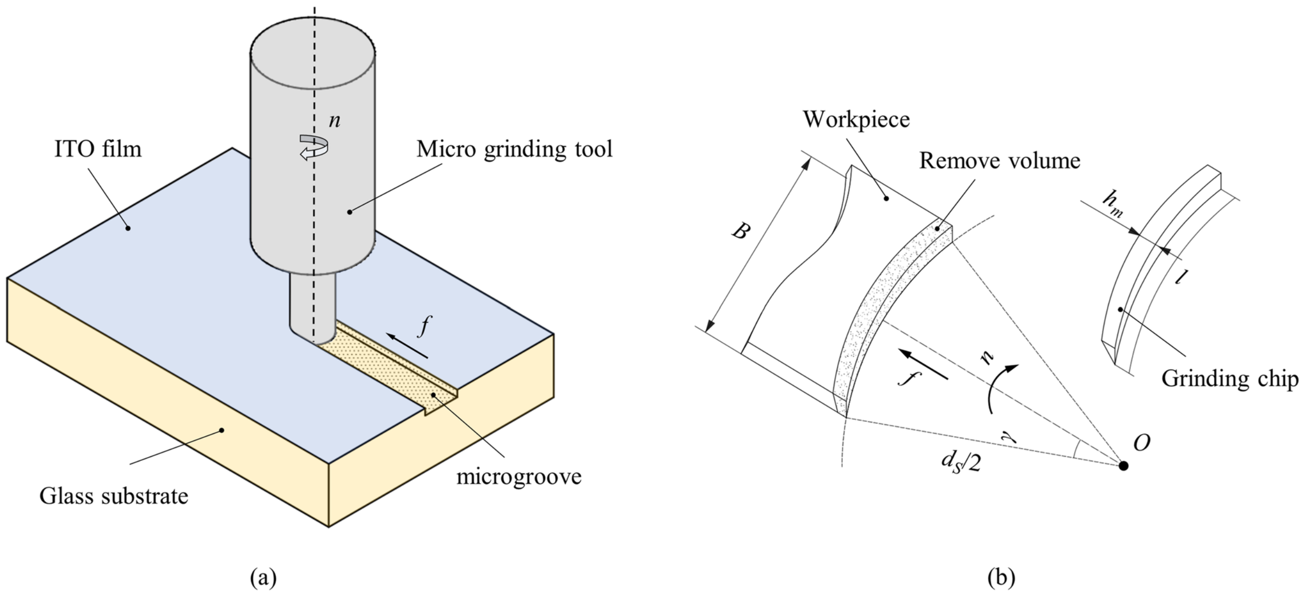


**Fig. 3** Schematic diagram of micro groove grinding. (**a**) Schematic diagram of microscale grinding of ITO conductive glass (**b**) Vertical plane grinding principle diagram

**Fig. 4** Geometric model of micro groove bottom grinding

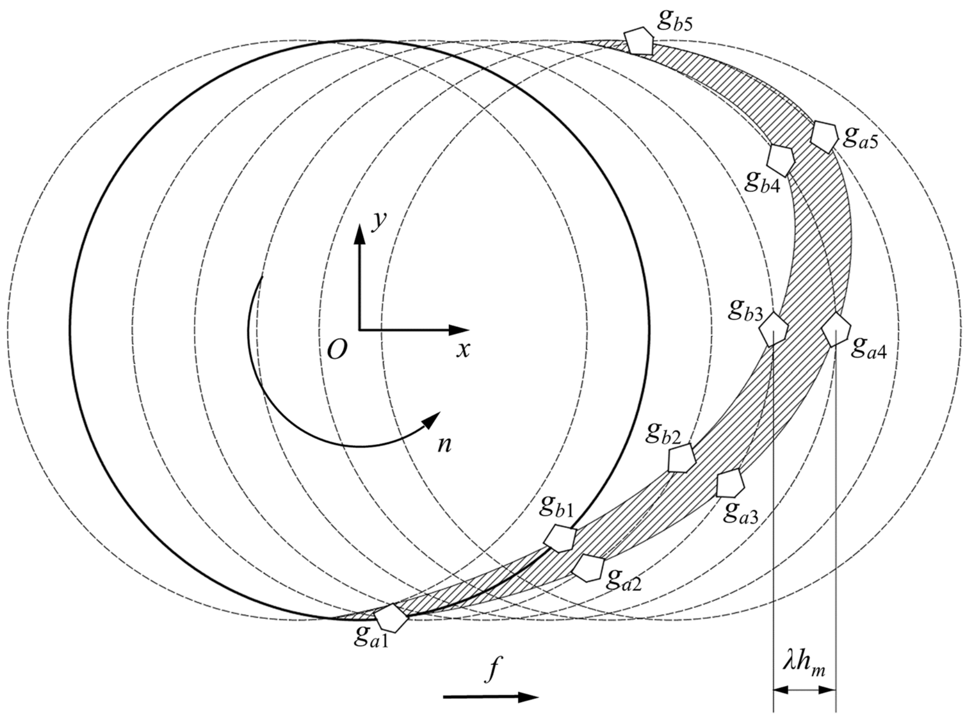


distance between $g_{a4}$ and $g_{b3}$, which can be expressed as follows:

$$\lambda h_m = ft = f\frac{l_g}{v_s} = f\frac{l_g}{d_s \pi n} \tag{13}$$

where $\lambda$ is the number of abrasive particles arranged per unit distance on the circumference and $l_g$ is the distance traveled by the grinding tool per unit time of the circumference.

According to the above formula, the maximum undeformed chip thickness for grinding the bottom of the micro groove can be expressed as follows:

$$h_m = \frac{M_d f l_g}{\lambda d_s \pi n} = \frac{M_d f}{C_d d_s \pi n} \tag{14}$$

where $C_d$ is the density of abrasive particles on the circumference of the microgrinding tool and $M_d$ is the microscale grinding size effect coefficient.

# 3 Removal mechanism of ITO conductive glass material

## 3.1 Film fracture mechanism

According to fracture mechanics, when a material is subjected to external loads, stress will concentrate at the crack tip, leading to crack propagation. When the material's characteristic strength is higher than the stress at the crack tip, the crack will be suppressed [23, 24, 25]. The total energy of the crack propagation system consists of elastic strain energy and load potential energy. In equilibrium, crack propagation causes the load potential energy to transform into elastic strain energy [26]. When the load potential energy is less than the unit fracture energy of the material, the crack no longer propagates.

To explain the mechanism of material fracture, Irwin proposed the concept of stress field intensity factor, which is used to describe the stress field intensity at the crack tip. When it is greater than the specific value of material fracture toughness, it indicates that the stress concentration at the crack tip is severe, which will lead to further crack propagation. The relationship between the energy release rate of crack propagation and the stress field intensity factor under quasi-static plane loading conditions is as follows:

$$G = \frac{1 - v^2}{E}(K_{\mathrm{I}}^2 + K_{\mathrm{II}}^2) \tag{15}$$

where $G$ is the energy release rate; $K_{\mathrm{I}}$ and $K_{\mathrm{II}}$ are, respectively, I type and II type the stress intensity factor of the fracture mode.

The failure of thin film composite materials mainly involves the propagation of microcracks under tension. At present, cohesive fracture and interface delamination are considered the main failure modes of thin film materials [27]. Cohesive fracture is the cracking of brittle films under tension, commonly known as channel fracture. And interface delamination is a buckling delamination caused by poor adhesion between the film and the substrate. For thin film composite materials composed of two uniform and isotropic materials, the relationship between the energy release rate of crack propagation at the plane interface and the stress field intensity factor can be expressed as:

$$G = \frac{E_f + E_s}{2E_f E_s}(K_{\mathrm{I}}^2 + K_{\mathrm{II}}^2) = \frac{1}{E_s\left(1 + D_1\right)}(K_{\mathrm{I}}^2 + K_{\mathrm{II}}^2) \tag{16}$$

where $D_1$ is the Dundurs parameter for the elongation stiffness of the thin film and substrate and $E_f$ and $E_s$ are, respectively, the elastic moduli of the thin film and the substrate.

In the process of material fracture, the energy required for crack propagation comes from surface energy and plastic deformation energy. For a single homogeneous material, cracks often propagate along paths with tensile stress states to minimize energy consumption [28]. When cracks propagate at the interface of thin film materials, the fracture work is affected by the tensile and shear stresses at the crack tip.

## 3.2 Film adhesion mechanism

Film adhesion refers to the bonding strength between the film and the substrate material at the contact surface, which is influenced by factors such as the properties of the film and substrate material and the film preparation process. For ITO conductive glass prepared by magnetron sputtering technology, the interlayer adhesion is mainly determined by the combined effects of van der Waals forces, electrostatic forces, and chemical adsorption.

During magnetron sputtering, high-energy ions bombard the surface of the target material, causing atoms or molecules on the target material to dissociate from the surface and deposit on the substrate, forming a thin film. The uneven distribution of electrons within the atoms of the thin film and substrate leads to the attraction caused by the instantaneous dipole moment of electrons, generating van der Waals forces between the two contact surfaces. The ion particles generated by magnetron sputtering have electrostatic charges. When the ions approach the surface of the substrate, their charges interact with the charges on the substrate, generating electrostatic forces. In addition, during magnetron sputtering, atoms or molecules on the target material interact with atoms or molecules on the substrate surface and form chemical bonds, thereby increasing the binding force.

The peeling of the film from the substrate will absorb energy to produce a new surface, thereby increasing the total energy of the system. The adhesion of the film is related to the surface free energy:

$$W = \gamma_f + \gamma_s - \gamma_{fs} \tag{17}$$

where $\gamma_f$ and $\gamma_s$ represents the surface free energy of the thin film and substrate, respectively, and $\gamma_{fs}$ is the interface free energy.

### 3.3 Material removal mechanism

The crack morphology generated by brittle material scratch test and indentation test is similar, and to some extent, scratch test can be regarded as a series of indentations along the direction of the scratch. The translation pressure head mainly affects the density of cracks generated by the material and has a relatively small impact on the depth of cracks. So, the removal of brittle materials during the grinding process can be analyzed using indentation and fracture theory.

Lateral cracks and median cracks are two typical main cracks in the indentation process of brittle materials [29]. Lambropoulos derived theoretical equations for the depth of lateral cracks and median cracks through indentation tests. The depth of median crack $c_m$ can be expressed as follows [30]:

$$c_m = \alpha_K^{2/3}\left(\frac{E}{H}\right)^{(1-m)2/3}(\cot\theta)^{4/9}\left(\frac{P}{K_c}\right)^{2/3} \tag{18}$$

The depth of lateral crack $c_l$ can be expressed as follows:

$$c_l = 0.43(\sin\theta)^{1/2}(\cot\theta)^{1/3}\left(\frac{E}{H}\right)^m\left(\frac{P}{H}\right)^{1/2} \tag{19}$$

where $m$ is a dimensionless constant, with a value range of 0.33 to 0.50 and $\alpha_K$ is a dimensionless parameter, while $\alpha_K = 0.027 + 0.090(m - 0.33)$.

When the indenter moves on the surface of the material, the scratch hardness $H_s$ is usually used as an indicator of the material's inherent resistance to scratch deformation, which can be expressed as follows [31]:

$$H_s = \frac{P}{A_N} = \beta\frac{P}{h_s^2}\cot^2\theta \tag{20}$$

where $A_N$ is the contact area of the normal projection of the indenter, $\beta$ is the elastic recovery coefficient of the material, and $h_s$ is the depth of penetration of the scratch.

By substituting formula (20) into formula (18), the expression for the median crack under scratch action can be obtained:

$$c_m = 0.206\left(\frac{E^{1/2}H_s^{1/2}}{K_c\beta}\right)^{2/3}(\tan\theta)^{8/9}{h_s}^{4/3} \tag{21}$$

According to the scratch elastic-plastic stress field model proposed by Jing et al. [32], it can be inferred that the median crack of brittle materials under scratch action can be represented as follows:

$$c_l = \left(\frac{3(1\text{-}2v)}{5-4v} + \frac{2\sqrt{3}}{\pi(5-4v)}\left(\frac{E}{H}\right)^{4/3}\cot\theta\right)^{1/2} h_s\tan\theta \tag{22}$$

As shown in Fig. 5, the material removal and surface formation caused by lateral cracks generated by abrasive particles during the grinding process determine the surface roughness *SR*. And the sub surface damage depth of the median diameter crack is *SSD*, so there are:

$$d_{SR} = c_m - h_s \tag{23}$$

$$d_{SDD} = c_l - h_s \tag{24}$$

Compared to the glass substrate, the material characteristic strength of the ITO film attached to it is relatively higher. During abrasive cutting, there is an elastic mismatch between the glass substrate and the ITO film, which can lead to cracks between the substrate and the film [33]. Meanwhile, due to the different damage intensities between the thin film layer and the substrate, the substrate will yield prematurely under the action of abrasive particles, and the thin film layer will generate stress concentration due to substrate deformation, further forming brittle fracture.

When the substrate glass material is removed by abrasive particles in the plastic deformation area, the

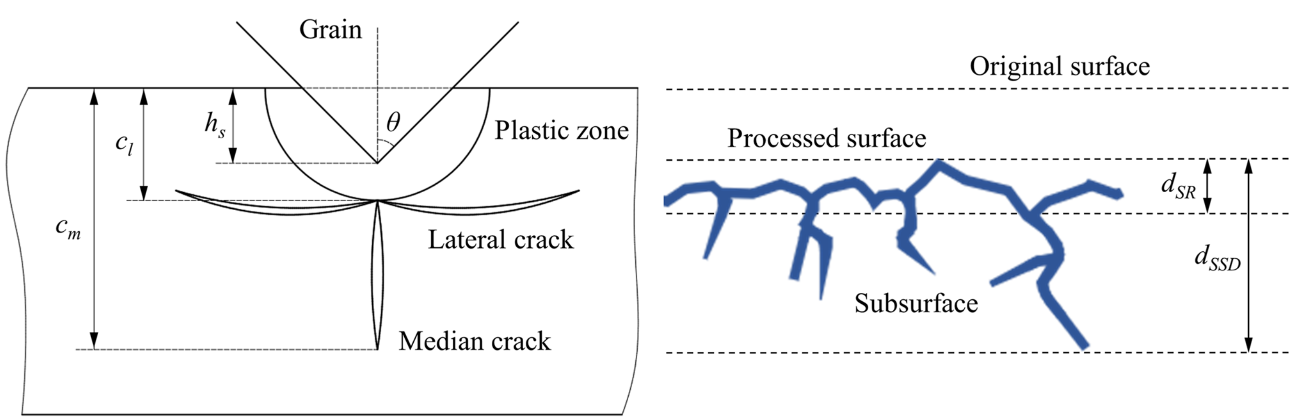


**Fig. 5** Crack evolution model

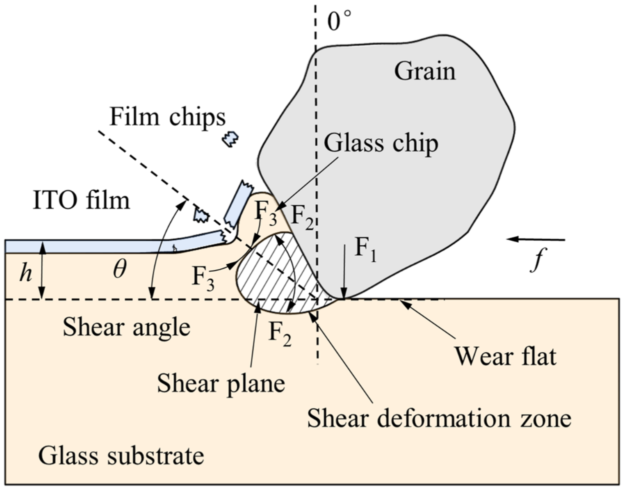


**Fig. 6** Removal mechanism of ITO conductive glass material

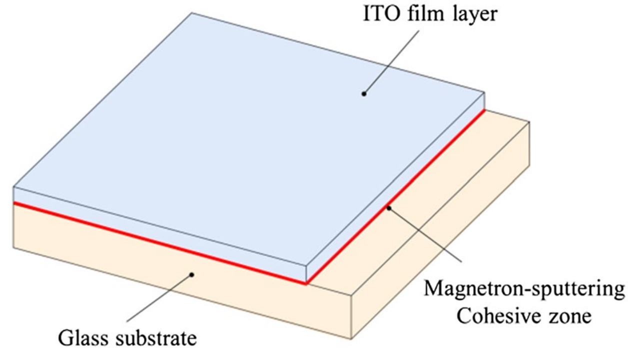


**Fig. 7** Structure diagram of ITO conductive glass

removal state of the film and substrate is shown in Fig. 6. At this time, the cutting depth of abrasive particles is much greater than the thickness of the film, but it has not reached the critical depth of brittle fracture of the glass substrate. The characteristic strength of the film is higher than that of the glass substrate, so the deformation of the substrate is restrained to a certain extent. Originally, the process of glass chips produced by plastic flow was hindered by the film. It makes the interface between the film and the substrate appear dislocation, and the film appears microcracks due to elastic mismatch. These cracks gradually extend under the action of abrasive particles, forming brittle fracture of the film.

## 4 Simulation of ITO glass single abrasive cutting

### 4.1 ITO glass material model

ITO conductive glass is a kind of film composite material. In the production process, the film layer is combined with the glass substrate through magnetron sputtering. The ITO conductive glass material model requires the definition of the film layer, substrate, and magnetic bonding region, as shown in Fig.7.

The material of the glass substrate is soda-lime glass, which is a typical brittle material. To characterize its mechanical behavior of large displacement and deformation during single abrasive cutting process, the Johnson-Holmquist Ceramic (JH-2) constitutive model is selected as the material model. Its basic expression is as follows:

$$\sigma^* = \sigma_i - D\left(\sigma_i - \sigma_f\right) \tag{25}$$

where $\sigma^*$ is the standardized equivalent stress, $D$ is the damage factor, $\sigma_i$ is standardized complete equivalent stress, and $\sigma_f$ is the standardized fracture equivalent stress.

The equivalent stress formula for material intact ($D=0$) is as follows:

$$\sigma_i = A(P^* + T^*)^N \left[1 + C \cdot \ln \dot{\varepsilon}^*\right] \tag{26}$$

The equivalent stress formula for material fracture ($D=1$) is as follows:

$$\sigma_f = B(P^*)^M \left[1 + C \cdot \ln \dot{\varepsilon}^*\right] \tag{27}$$

where $A$, $B$, $C$, $M$, and $N$ are material strength parameters, $P^*$is the standardized compressive strength, $T^*$ is the standardized tensile strength, and $\dot{\varepsilon}^*$ is the strain rate.

The equation of state for the material model is as follows:

$$P = K_1\mu + K_2\mu^2 + K_3\mu^3 \tag{28}$$

where $P$ is the hydrostatic pressure; $K_1$, $K_2$, and $K_3$ are material constants; and $\mu$ is the volumetric strain.

The specific JH-2 constitutive parameters for the glass substrate are shown in Table 1 [34].

Brittle cracking is a model used to simulate brittle cracking in materials, often utilized in the study of particle-reinforced composite materials failure mechanisms. The ITO film layer adopts the brittle cracking model to represent its brittle failure form. When the maximum normal stress acting on the ITO film exceeds its tensile strength, the film elements begin to fracture, and the subsequent crack evolution displacement is as follows:

$$u_n = \frac{2G_f^{\mathrm{I}}}{\sigma_t} \tag{29}$$

where $G_f^{\mathrm{I}}$ is the I-type fracture energy of the ITO film and $\sigma_t$ is the tensile strength of the material.

**Table 1** JH-2 parameters of glass substrate

| Parameter | | Value |
|---|---|---|
| Density $\rho$(kg/m$^3$) | | 2690 |
| Shear modulus $G$(MPa) | | 2690 |
| Damage constants | $D_1$ | 0.043 |
| | $D_2$ | 0.85 |
| | $FS$ | 1.0 |
| State constants | $K_1$ | 43.2 |
| | $K_2$ | -67.2 |
| | $K_3$ | 153.2 |
| Strength constants | $A$ | 0.71 |
| | $B$ | 0.178 |
| | $C$ | 0.01833 |
| | $M$ | 1 |
| | $N$ | 0.61 |
| | $T$ | 27.8 |
| | $HEL$(MPa) | 5950 |
| | $P_{HEL}$(MPa) | 2920 |
| | $S_{FMAX}$(MPa) | 0.5 |

The shear modulus at the cracking stage of ITO film layer is:

$$G_c = \rho\left(e_{nn}^{ck}\right)G \tag{30}$$

where $G$ is the shear modulus of the film before cracking and $\rho\left(e_{nn}^{ck}\right)$ is the shear retention factor, which is calculated as follows:

$$\rho\left(e_{nn}^{ck}\right) = \left(1 - \frac{e_{nn}^{ck}}{e_{\max}^{ck}}\right)^p \tag{31}$$

where $\mathrm{e}_{\mathrm{nn}}^{\mathrm{ck}}$ is the crack opening strain $\mathrm{e}_{\max}^{\mathrm{ck}}$ and $p$ is the material parameter.

The material properties of ITO films are shown in Table 2 [35].

In the study of interface damage in composite materials, a cohesive model is commonly used to simulate interlayer failure form [36]. This paper establishes a cohesive behavior in the magnetron-sputtering cohesive zone between the ITO film and glass substrate to characterize the delamination, crack, and other mechanical behaviors of the material during abrasive cutting. The cohesive model is shown in Fig. 8.

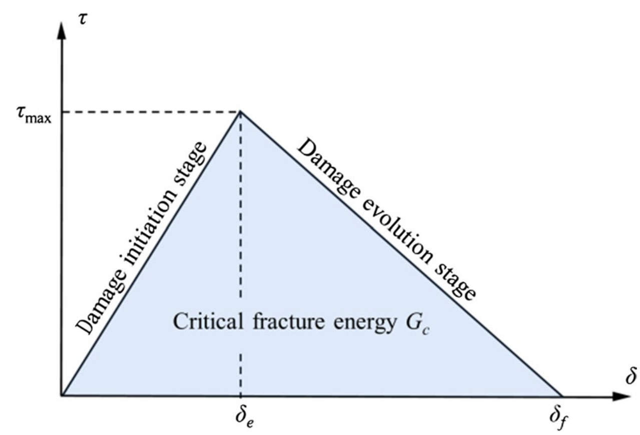


**Fig. 8** Model of cohesive zone

At the damage initial stage, the tension-displacement relationship is linear elastic, and the expression of the cohesive model relationship can be shown as follows:

$$\tau = K\delta \tag{32}$$

where $\tau$ is tension, $\delta$ *is* separation displacement, $K$ is the stiffness of cohesive zone, and the calculation formula is as follows:

$$K = \frac{E}{H_{eff}} \tag{33}$$

where $E$ is the modulus of cohesive zone and $H_{\mathrm{eff}}$ is the effective thickness of cohesive zone.

According to the secondary stress criterion, the damage evolution stage begins when the stress reaches the initial damage criterion. The damage evolution stage ends when the energy release rate reaches the critical value, where the critical fracture energy is numerically equal to the area enclosed by the tension-displacement curve:

$$G_c = \frac{1}{2} \cdot \delta_f \cdot \tau_{\max} \tag{34}$$

where $G_c$ is the critical fracture energy, $\delta_f$ is the maximum crack opening displacement, and $\tau_{\max}$ is the initial stress of the damage.

**Table 2** Material properties of ITO films

| Density $\rho$(kg/m$^3$) | Young's modulus $E$(GPa) | Poisson's ratio $v$ | Tensile strength $\sigma_t$(MPa) | Fracture energy $\mathrm{G}_\mathrm{f}^\mathrm{I}$/(J/m$^2$) |
|---|---|---|---|---|
| 6800 | 116 | 0.35 | 293 | 36.3 |

## 4.2 Simulation analysis

In the single abrasive cutting simulation of ITO conductive glass, Fig. 9 shows the stress nephogram with a cutting depth of 0.4 μm and a cutting speed of 2500 mm/s. It can be seen that the cutting marks left by the abrasive

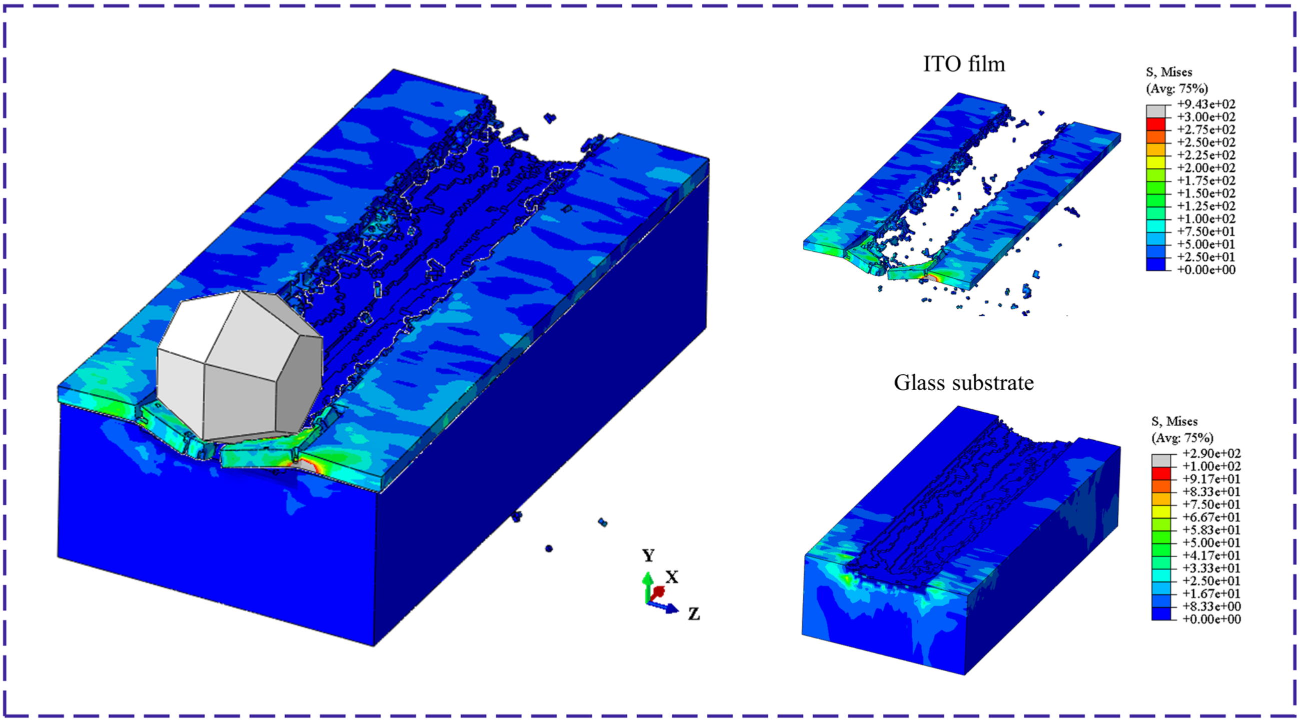


**Fig. 9** Stress nephogram of abrasive cutting ITO conductive glass

particles on the surface of the workpiece are mainly determined by the shape of the abrasive particles entering the workpiece. During the cutting process, stress is mainly concentrated in the front contact area between the workpiece and abrasive particles. When the ITO film reaches the damage strength, the film unit fails and is removed. The grains of the brittle film material shatter into smaller particles, which are removed in the form of powder. There is a certain residual stress at the edge of the cut, which is caused by the elastic mismatch between the thin film layer and the glass substrate.

In order to facilitate the observation of the machining surface morphology, the ITO thin film layer is displayed separately. At this moment, there are a large number of “burrs” at the edge of the cutting mark. This is because the ITO thin film unit at the edge of the cutting mark did not meet the damage standard during cutting, but the glass unit on the substrate was already damaged in advance. Under the compression of the abrasive particles, stress concentration occurred at the edge of the thin film, leading to the removal of brittle fracture during the cutting process. Therefore, the morphology of the cutting mark is relatively rough. When the glass substrate is displayed separately, the stress in the thin layer is transmitted to the substrate. At the same time, due to microscale abrasive cutting, the plastic deformation of the glass caused by its tip leads to the formation of a circular stress concentration area in front of the abrasive tip of the glass substrate. This will cause the glass unit to reach the damage criterion ahead of time without contact with the abrasive, resulting in sub surface damage during material processing.

Figure 10 shows the stress morphology of the ITO film and glass substrate during the cutting stage of the abrasive particles. As the abrasive particles reach the edge of the workpiece, the cohesive contact between the lower layers under the action of grinding force reaches the failure criterion, and the film and substrate gradually layer by layer. The thin film unit in contact with the abrasive blade gradually cracks, causing cracks to appear on the thin film layer. During the abrasive cutting process, the glass units on the thin film substrate deform too much and are damaged prematurely, resulting in interlayer cracks. The thin films on both sides in front of the abrasive particles are subjected to oblique downward forces, causing brittle cracking of the films and the formation of channel cracks. Under the action of abrasive particles, cracks on the thin film layer gradually penetrate, forming interfacial fractures within and between the thin film layers. Flaky thin film chips are gradually peeled off, and the cutting force of the abrasive particles in the subsequent stage is significantly reduced. As the abrasive particles are cut out, the sheet-like film chips separate from the substrate, and under the compression of the abrasive particles, the glass substrate at the edge of the workpiece is damaged.

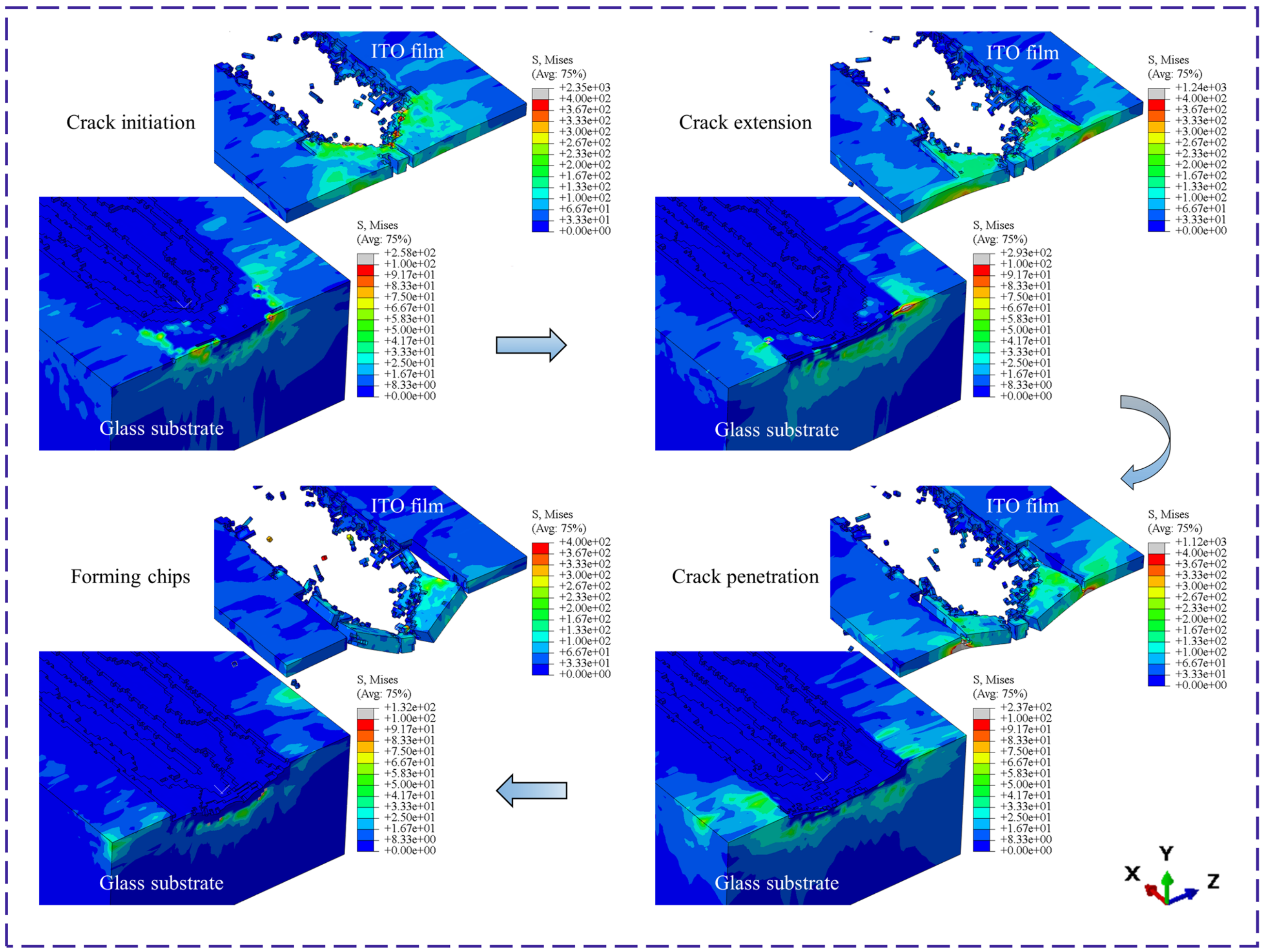


Fig. 10 Stress nephogram of ITO conductive glass material

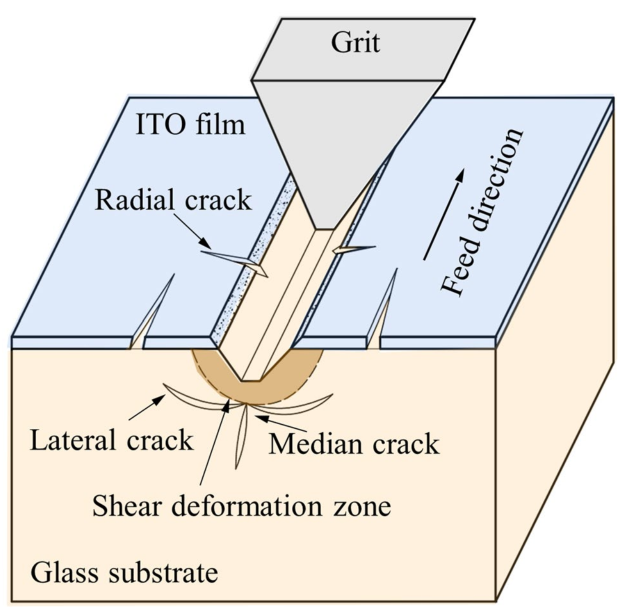


Fig. 11 Principle diagram of abrasive cutting ITO conductive glass

As shown in Fig. 11, the material strength of the ITO thin film layer itself is higher, and during abrasive cutting, it will hinder the shear deformation of the substrate and compress the shear deformation zone. However, the shear deformation of the glass substrate leads to an elastic mismatch between the film and the substrate, which in turn can cause delamination between the film and the substrate, and even crack the film. Due to the high elastic modulus and thin thickness of ITO film, it is in a brittle fracture removal state during the cutting process of abrasive particles. The cracks in the film are extended to the point of penetration by the action of abrasive particles, resulting in large brittle chips. When the cutting depth of the abrasive increases, the glass substrate will transition from material removal to brittle removal, resulting in medium diameter cracks and transverse cracks at the edge of the plastic deformation zone of the glass substrate.

Soda-lime glass is the substrate material of ITO conductive glass. Figure 12 shows the variation curve of tangential force with cutting time for ITO conductive glass and soda-lime glass under the same cutting

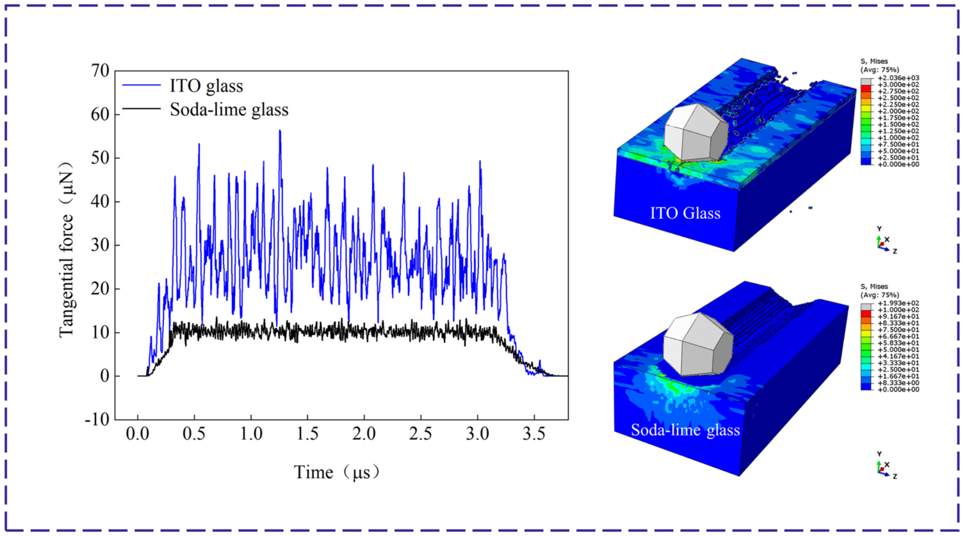


**Fig. 12** Comparison of cutting forces between two materials

parameters of a single abrasive. It can be seen that the cutting force value of ITO conductive glass is larger and fluctuates more violently throughout the entire cutting process, which is due to the high elastic modulus and high hardness of ITO thin films. This difference is mainly due to the fact that the cutting depth of the abrasive particles is close to the thickness of the thin film, and the effect of the thin film is more obvious. As the cutting depth increases, the effect of the thin film on cutting force will gradually decrease. It can be clearly stated that the presence of thin films enhances the material characteristic strength of the original material surface, making the material more wear-resistant and difficult to process.

## 5 ITO glass microgrinding experimental equipment

As shown in Fig. 13a, the microscale grinding experiment of ITO conductive glass was conducted on the VMC5640V4 machine tool, and the MC3D160 dynamometer was fixed on the machine tool using a vacuum chuck. As shown in Fig. 13b, the tool used for microscale grinding is a cylindrical grinding tool with a diameter of 0.9 mm and electroplated 500 # diamond. The surface morphology of the grinding tool is shown in Fig. 13c. Install the test workpiece on the force measuring instrument using a dedicated fixture and collect the mechanical signals during the machining process in real time through the MCD3USB signal acquisition card.

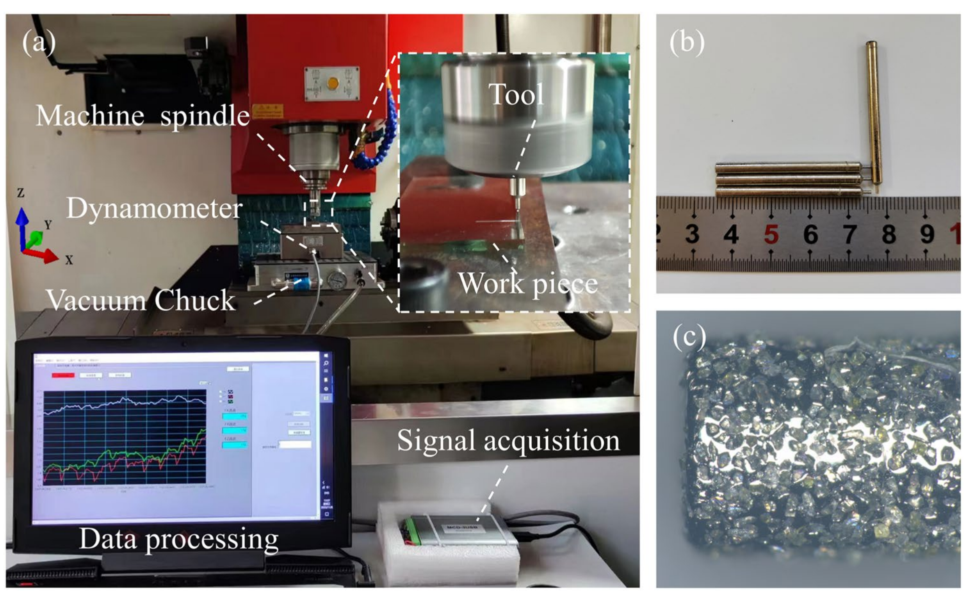


**Fig. 13** Experimental platform and machining tools. (**a**) Experimental platform (**b**) Microscale grinding tools (**c**) morphology of micro-grinding tool

**Fig. 14** Workpieces of ITO conductive glass

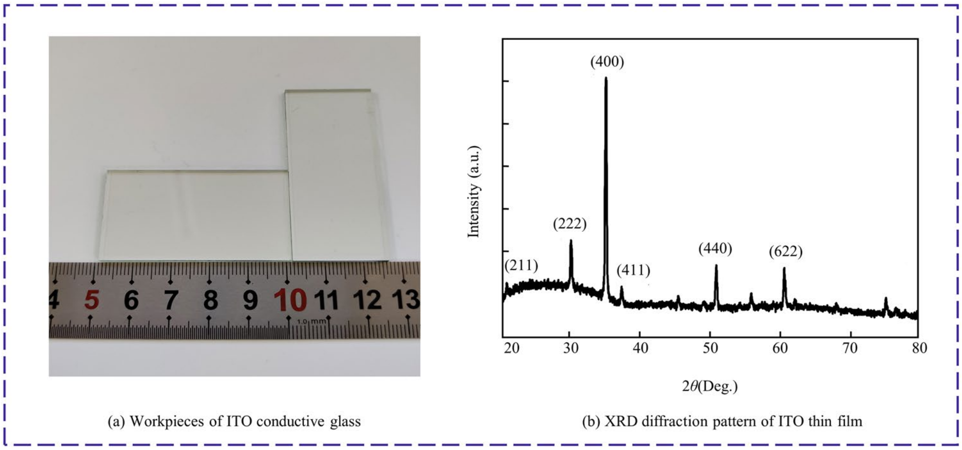


**Fig. 15** Micro grooves on the workpiece

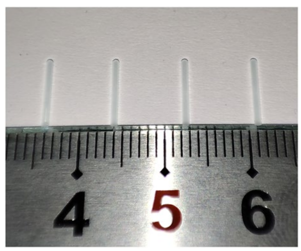


The ITO conductive glass used in this experiment is shown in Fig. 14a, with a workpiece size of 25×50×2 mm, with a thin film layer thickness of 0.2 μm. The original square resistance of the thin film is about 6.8 Ω. Figure 14b shows the XRD diffraction pattern of the ITO film on a glass substrate. In the pattern, there are peaks on the (211), (222), (400), (440), and (622) crystal planes of $In_2O_3$, indicating that the ITO film deposited by magnetron deposition is currently in a crystalline state.

## 6 Analysis and discussion

Figure 15 shows the microgrooves obtained from microgrinding experiments on the surface of ITO conductive glass workpieces. A cylindrical microgrinding tool was used to grind the workpiece, resulting in a microgroove diameter of approximately 0.9 mm. In order to facilitate subsequent measurement of the length of the cutting micro groove, which is slightly 8 mm, the processed microgrooves are evenly spaced.

The fluctuation curve of the tangential force of the grinding tool during micro groove grinding of ITO conductive glass and soda-lime glass is shown in Fig. 16a. In the stable microgrinding process with the same processing parameters, the tangential grinding forces of both materials are within a certain range, but the presence of thin films makes the grinding force of ITO conductive glass greater than that of soda-lime glass. The minimum values of the two curves are close, but the difference between the maximum values is large, indicating that the characteristic strength of the thin film material is higher. The brittle fracture during the grinding process causes certain fluctuations in the grinding force and can affect the removal state of the substrate material during the grinding process.

In the experiment, soda-lime glass was set as the control group, and the surface morphology of the micro grooves was captured using a superdepth microscope. The results are shown in Fig. 16b, (c). Comparing the two images, it can be observed that the surface of ITO conductive glass microgrooves with thin films has more dense defects and cracks, with darker colors in the images.

Due to the high material characteristic strength of ITO film, the presence of the film suppresses the shear deformation of the substrate glass, resulting in a greater cutting force required by the abrasive particles during the cutting process. The plastic deformation of the glass substrate is suppressed, causing accumulation at the interface between the film and substrate, resulting in cracks in the film. At the same time, the elastic mismatch between the interfaces causes high temperatures in the friction between the glass substrate and the grinding tool, further leading to more cracks, micropits, and burns on the surface of the microgrooves.

In the machining process of microgrooves, the effect of the grinding tool can be regarded as the collaborative cutting of multiple cutting edges on the workpiece. Therefore, studying the motion trajectory of the abrasive particles can understand the interaction between the abrasive particles and the workpiece during the grinding process.

As shown in Fig. 17, based on the contact state between the abrasive particles and the workpiece during micro-scale grinding, kinematic analysis is performed on a single abrasive particle. The center position of the bottom surface of the grinding tool is set as the coordinate origin $O$, and the microgrinding tool is defined to feed along the $X$ direction. If

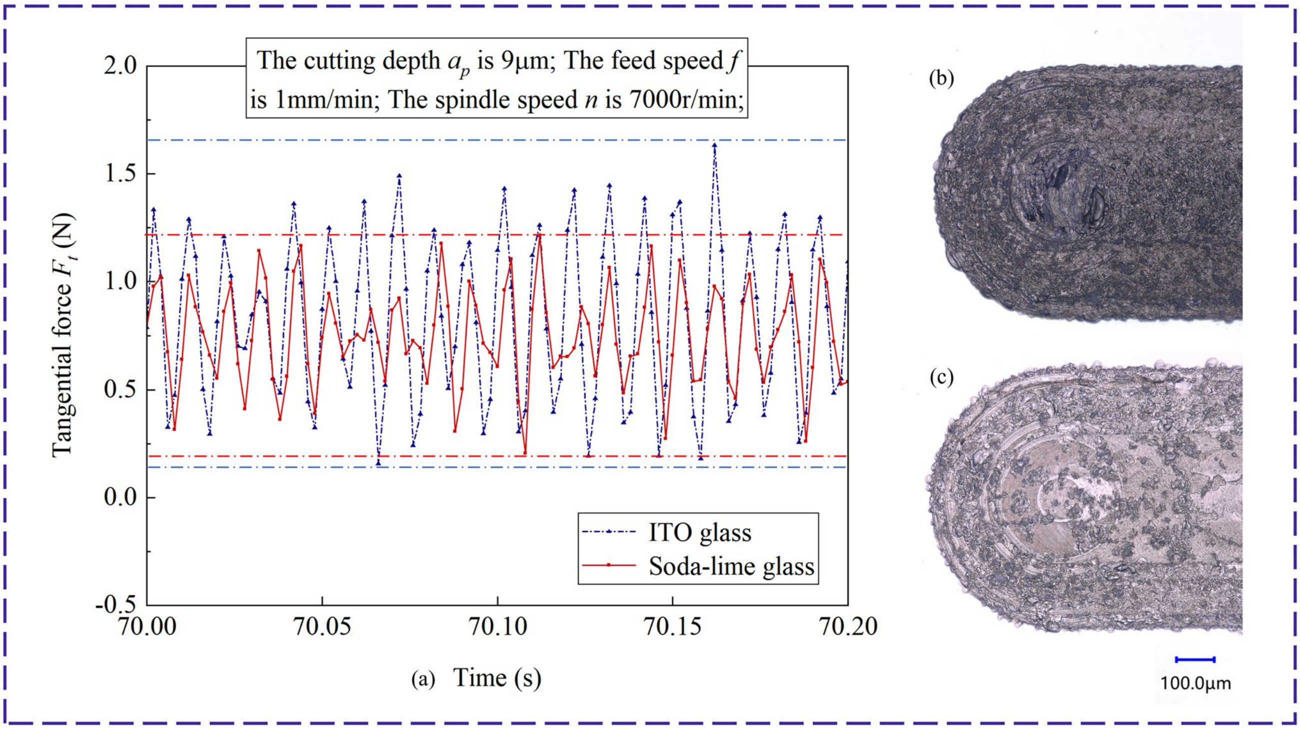


**Fig. 16** Comparison of microgrinding of two materials. (**a**) Tangential force fluctuation curve of micro grinding (**b**) Surface morphology of ITO glass (**c**) Surface morphology of soda-lime glass

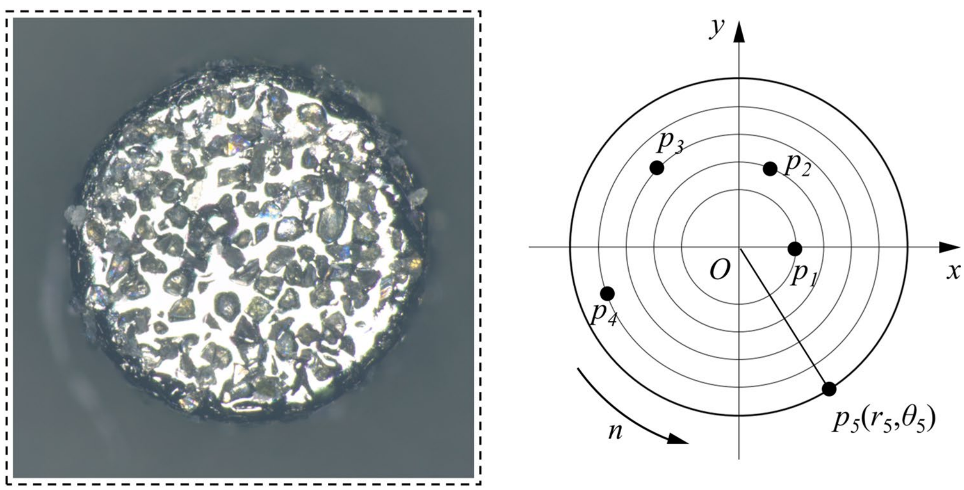


**Fig. 17** Definition of abrasive particle position

the polar coordinate $p_i$ ($r_i$, $\theta_i$) is used to represent the initial positions of each abrasive particle, the motion trajectory of the abrasive particle can be defined as follows [37]:

$$\begin{cases} x_i = \frac{f \cdot t}{60} + r_i \cos\left(\frac{2\pi nt}{60} + \theta_i\right) \\ y_i = r_i \sin\left(\frac{2\pi nt}{60} + \theta_i\right) \end{cases} \tag{35}$$

where $n$ is the spindle speed, $f$ is the feed speed of the grinding tool, and $i$ is the abrasive particle number.

According to the polar coordinates of each abrasive particle on the end face of the microgrinding tool set in Fig. 17, define the process parameters for microscale grinding, and substitute them into formula (35) to obtain the specified abrasive particle motion trajectory. As shown in Fig. 18, the morphology of the abrasive trajectory is determined by the feed rate $f$ and the spindle speed $n$, which together determine the distribution state of the abrasive trajectory in the coordinate system.

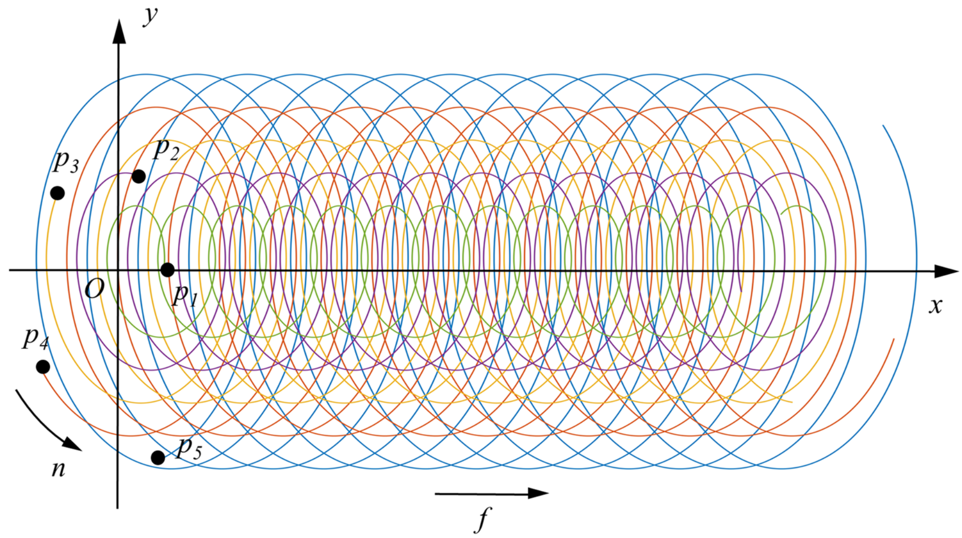


**Fig. 18** Model of abrasive particle motion trajectory

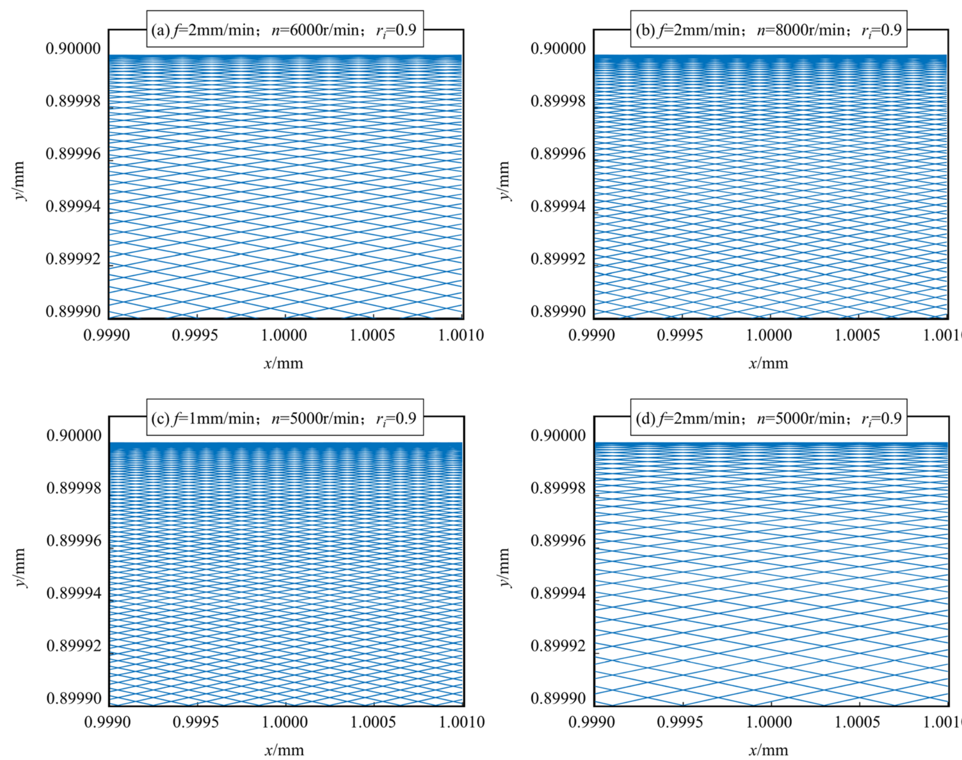


**Fig. 19** Distribution of abrasive particle trajectories under different process parameters

Figure 19 shows the trajectory of abrasive particles with an initial position of $p_5$ ($r_5$, $\theta_5$) under actual machining parameters. The limited coordinate area in the figure displays the distribution of abrasive particle trajectories at the edge of the micro groove. Comparing Fig. 19a, b, the influence of rotational speed on the distribution of abrasive particle trajectories can be analyzed. Increasing rotational speed will make the distance of abrasive particles passing through the surface of the workpiece longer per unit time of feed distance, thereby making the trajectory distribution more dense. Compared to Fig. 19a, it can be observed that there are more overlapping areas of serrated trajectories at the edges of the abrasive trajectory in Fig. 19(b). Compared to other areas, increasing the rotational speed makes the grinding of the edges more thorough by the abrasive particles. It can be inferred from this that the abrasive particles at the edge of the microgrinding tool affect the lateral quality of microgroove grinding, and the damage state of the edge abrasive particles has a significant impact on the lateral grinding quality of microgrooves, which is an important reason for the occurrence of edge crack in microgrooves.

By comparing Fig. 19(c) with Fig. 19(d), the influence of feed rate on the distribution of abrasive trajectory can be analyzed. Reducing the feed rate makes the cutting of the workpiece more thorough by the abrasive particles, and the distribution of abrasive particle trajectories becomes more dense, thereby improving the machining quality of the surface. At the same time, a lower feed rate will also increase the overlap area of abrasive trajectory edges, improving the grinding quality of micro groove edges.

Figure 20 shows the surface morphology of micro grooves under two different removal states, where Fig. 20a shows the surface morphology of ductile and brittle removal modes coexisting. Microgrooves have defects such as brittle cracks, and there are also residual grinding chips in the grooves. These chips are embedded in the machining surface, leaving micro pits that affect the machining quality. When the feed rate is fast and the spindle speed is low, the undeformed chip thickness of micro grinding is greater than the critical cutting thickness, and the abrasive particles compress the workpiece to produce transverse cracks. This crack further extends and forms the brittle removal of the material. When the feed rate is reduced and the spindle speed is increased, the undeformed chip thickness of micro grinding is less than the critical cutting thickness, and the removal of abrasive particles from the workpiece is within the plastic range of the material. At this point, the material is in a ductile removal state.

In Fig. 20b, ductile deformation and other morphologies can be observed on the surface of the micro groove. At this time, the glass material of the substrate is in a ductile removal state. Compared with Fig. 20a, the edge crack in this state is smaller, and the overall serrated shape appears at the edge of the micro groove. Comparing the distribution of abrasive particle trajectories in Fig. 19, it can be found that the serrated edge crack is related to the distribution of abrasive particle trajectories at the edge of the micro grinding tool. The ITO film is in a brittle fracture removal mode under microscale grinding due to its small thickness, but the amount of edge fracture and edge crack is related to the cutting thickness of the abrasive particles.

By using a superdepth microscope to observe two micro grooves, Fig. 20c shows the processing morphology of the glass substrate under ductile brittle removal mode. It can be observed that the medium diameter cracks generated by abrasive particle compression cause subsurface damage to the glass substrate. Figure 2d shows the processing morphology of the glass substrate under ductile removal mode, with higher surface quality. Its surface exhibits morphological characteristics under ductile removal mode. In addition, it

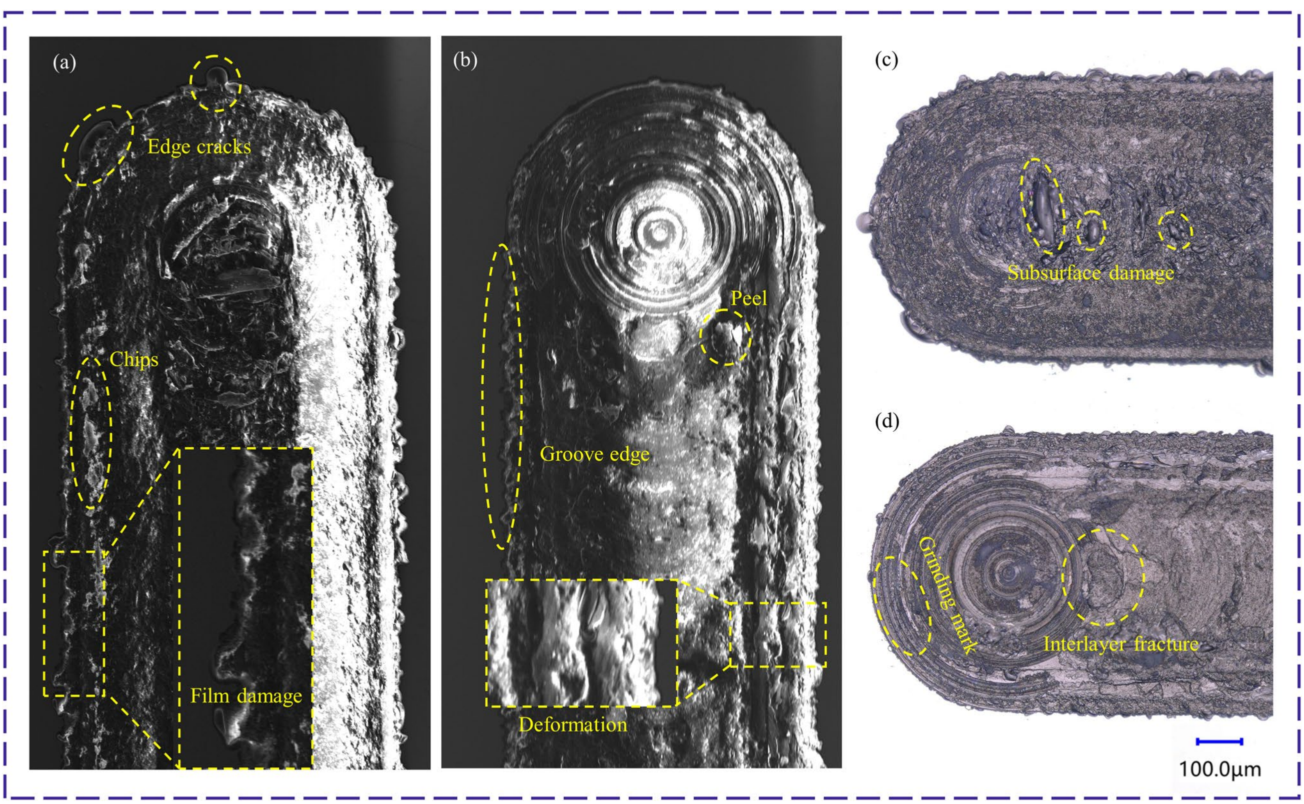


**Fig. 20** Microgrinding morphology of ITO glass. (**a**) SEM of substrate ductile–brittle removal mode (**b**) SEM of substrate ductile removal mode (**c**) Micro groove micrograph of ductile–brittle removal mode (**d**) Micro groove micrograph of ductile removal mode

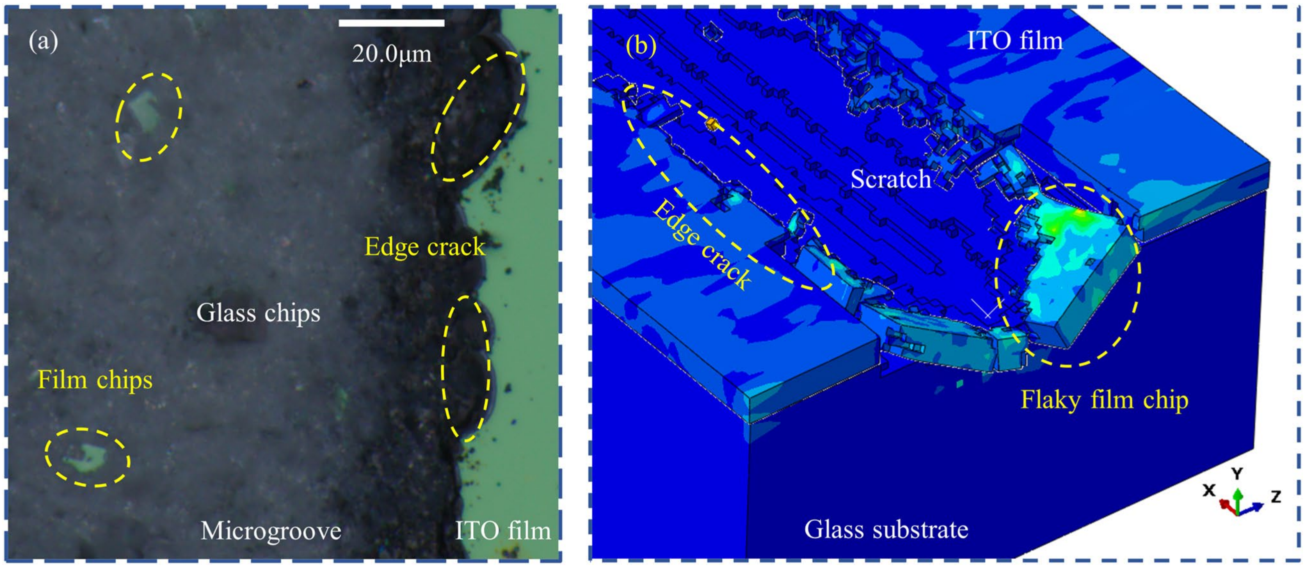


**Fig. 21** Micro grooves on the workpiece; (**a**) Edge crack and chips in micro groove; (**b**) Edge crack and chips in simulation

can be observed that the interface damage characteristics between the thin film and the glass substrate during the grinding process are due to the presence of the thin film.

Figure 21a shows the microgrooves obtained by microscale grinding and the morphology of chips generated during the micro grinding process. It can be observed that brittle fractures occur in the thin film at the edge of the microgrooves. At the same time, transverse cracks are generated on the glass substrate under the action of abrasive particles, and the cracks extend and penetrate, resulting in interlayer fractures between the thin film and substrate. This is consistent with the simulation results of single abrasive cutting in Fig. 21b. During grinding, ITO conductive glass chips mainly appear in two forms: flaky thin film chips and powder glass chips.

## 7 Conclusions

(1) In the microscale grinding process of ITO conductive glass, due to the small characteristic thickness of the thin film layer, it is always removed in a brittle fracture manner during the processing. When the thickness of the unmodified chips in micro grinding is less than the critical cutting thickness of the thin film material, the glass substrate removal state will transition to ductile removal.

(2) The structure of thin film composite materials based on ITO conductive glass adopts JH-2 constitutive model as the material model of the glass substrate, Brittle Cracking model as the material model of ITO thin film, and Cohesive behavior contact model to simulate the interlayer bonding form. The model established based on this can simulate the material removal state during the machining process.

(3) The material characteristic strength of ITO film is higher than that of glass substrate. The film layer can suppress the plastic deformation of the substrate during grinding, increasing the grinding force. At the same time, the brittle fracture of the film makes the fluctuation of grinding force more severe.

(4) The chips of ITO conductive glass are composed of flaky film chips and powder glass chips, and interlayer fracture is the main reason for the generation of flaky film chips.

**Author contribution** All authors contributed to the study conception and design. Material preparation, data collection, and analysis were performed by Xiaolong Qiu and Yin Liu. The first draft of the manuscript was written by Xingwei Sun, Xiaolong Qiu, and Yin Liu. Experimental tests were carried out by Xiaolong Qiu. All authors read and approved the final manuscript.

**Funding** This research was supported by the National Natural Science Foundation of China (Grant No. 52005346 and 52005347), Natural Science Foundation of Liaoning Province (Grant No. 2021-BS-149), Project of Liaoning Province Applied Basic Research Program (Grant No. 2022JH2/101300214), and General Project of Basic Scientific Research Projects for Higher Education Institutions of Liaoning Provincial Department of Education (Grant No. LJKMZ20220459).

## Declarations

**Consent for publication** The authors consent to publish this article.

**Competing interests** The authors declare no competing interests.

**Ethics approval** Not applicable.

**Consent to participate** Not applicable.

## References

1. Lewis BG, Paine DC (2000) Applications and processing of transparent conducting oxides. MRS Bull 25(8):22–27
2. Oh SJ, Kwon JH, Lee S et al (2021) Unveiling the annealing-dependent mechanical properties of freestanding indium tin oxide thin films. ACS Appl Mater Interfaces 13(14):16650–16659
3. Qu ZL, Zhang Q, He RJ et al (2017) Characterization of oxidation film on SiC ceramic substrate based on indentation method. Ceram Int 43(5):4399–4404
4. Wang ZX, Wang SB, Wang JR et al (2021) Mechanical performance of ITO/Ag/ITO multilayer films deposited on glass substrate by RF and DC magnetron sputtering. Ceram Int 47(22):31442–31450
5. Hengst C, Menzel SB, Rane GK et al (2017) Mechanical properties of ZTO, ITO, and a-Si:H multilayer films for flexible thin film solar cells. Materials 10(3):245
6. Feng ZD, Zhou YH, Tan R et al (2018) Dynamic damage and fracture of a conductive glass under high-rate compression: a synchrotron based study. J Non-cryst Solids 49440–49449
7. Zhu DH, Yan SJ, Li BZ (2014) Single-grit modeling and simulation of crack initiation and propagation in SiC grinding using maximum undeformed chip thickness. Comput Mater Sci 9213–9221
8. Lin XH, Ke XL, Ye H et al (2017) Investigation of surface/subsurface integrity and grinding force in grinding of BK7 glass. Proceedings of the Institution of Mechanical Engineers Part C-Journal of Mechanical Engineering Science 231(12):2349–2356
9. Ma LJ, Yu AB, Chen J (2017) Theoretical model of cutting force in turning the lithium disilicate glass-ceramic. Int J Adv Manuf Technol 92(9–12):4355–4366
10. Zhang XH, Kang ZX, Li S et al (2019) Grinding force modelling for ductile-brittle transition in laser macro-micro-structured grinding of zirconia ceramics. Ceram Int 45(15):18487–18500
11. Yang X, Qiu ZJ, Wang YG (2019) Investigation of material flow behaviour and chip formation mechanism during grinding of glass-ceramics by nanoscratch. Ceram Int 45(13):15954–15963
12. Sun Y, Su ZP, Gong YD et al (2020) An experimental and numerical study of micro-grinding force and performance of sapphire using novel structured micro abrasive tool. Int J Mech Sci 181
13. Tian L, Fu Y, Xu J et al (2015) The influence of speed on material removal mechanism in high speed grinding with single grit. Int J Mach Tools Manuf 89192–89201
14. Zhang Q, To S, Zhao Q et al (2016) Surface generation mechanism of WC/Co and RB-SiC/Si composites under high spindle speed grinding (HSSG). Int J Refract Met Hard Mater 56123–56131
15. Huang S, Gao S, Huang C et al (2022) Nanoscale removal mechanisms in abrasive machining of brittle solids. Diam &Abrasives Eng 42(3):257–267
16. Liu Y, Li J, Zhao Z et al (2024) Advanced grinding technologies for silicon carbide ceramic: a review. J Adv Manuf Sci Technol 4(1):2023016
17. Cheng J, Gong YD (2014) Experimental study of surface generation and force modeling in micro-grinding of single crystal silicon considering crystallographic effects. International Journal of Machine Tools & Manufacture 771 – 15
18. Piao YC, Li C, Hu Y et al (2024) Nanoindentation induced anisotropy of deformation and damage behaviors of MgF2 crystals. J Mater Res Technol 28:4615–4625
19. Soundararajan V, Radhakrishnan V (1986) An experimental investigation on the basic mechanisms involved in ultrasonic machining. Int J Mach Tool Des Res 26(3):307–321
20. Wang Y, Lin B, Wang SL et al (2014) Study on the system matching of ultrasonic vibration assisted grinding for hard and brittle materials processing. Int J Mach Tools Manuf 7766–7773
21. Yang YY, Yang M, Li CH et al (2023) Machinability of ultrasonic vibration-assisted micro-grinding in biological bone using nanolubricant. Front Mech Eng 18(1)
22. Srihari G, Lal GK (1994) Mechanics of vertical surface grinding. J Mater Process Technol 44(1):14–28
23. Qu SS, Yao P, Gong YD et al (2022) Environmentally friendly grinding of C/SiCs using carbon nanofluid minimum quantity lubrication technology. J Clean Prod 366:132898
24. Qu SS, Wei CX, Yang YY et al (2024) Grinding mechanism and surface quality evaluation strategy of single crystal 4H-SiC. Tribol Int 194:109515
25. Li C, Hu YX, Wei ZZ et al (2024) Damage evolution and removal behaviors of GaN crystals involved in double-grits grinding. Int J Extrem Manuf 6:025103
26. Yang YY, Gong YD, Li CH et al (2021) Mechanical performance of 316 L stainless steel by hybrid directed energy deposition and thermal milling process. J Mater Process Technol 291
27. Ziaei S, Wu Q, Fitch J et al (2019) Channel cracking and interfacial delamination of indium tin oxide (ITO) nano-sized films on polyethylene terephthalate (PET) substrates: experiments and modeling. Exp Mech 59(5):703–712
28. Wu M, Wang C, Zheng L et al (2022) Research on grinding of biological tissue. Diam Abrasives Eng 42(2):137–149
29. Lv B, Lin B, Cao Z et al (2024) Damage and crack extension mechanism of hard and brittle materials induced by cyclic indentation. J Adv Manuf Sci Technol 4(2):2024003
30. Lambropoulos JC, Li Y, Funkenbusch PD et al (1999) Noncontact estimate of grinding-induced subsurface damage. Proceedings of SPIE - The International Society for Optical Engineering 378241-50
31. Gu W, Yao Z, Li H (2011) Investigation of grinding modes in horizontal surface grinding of optical glass BK7. J Mater Process Tech 211(10):1629–1636
32. Jing X, Maiti S, Subhash G (2010) A new analytical model for estimation of scratch-induced damage in brittle solids. J Am Ceram Soc 90(3):885–892
33. Hsu J-S, Lee C-C, Wen B-J et al (2016) Experimental and simulated investigations of thin polymer substrates with an indium tin oxide coating under fatigue bending loadings. Materials 9(9):720
34. Tan S, Long S, Yao X et al (2021) An improved material model for loading-path and strain-rate dependent strength of impacted soda-lime glass plate. Journal of Materials Research and Technology-Jmr&T, pp 151905–151919
35. Chen J, Bull SJ (2006) Assessment of the toughness of thin coatings using nanoindentation under displacement control. Thin Solid Films 494(1–2):1–7
36. Harper PW, Hallett SR (2008) Cohesive zone length in numerical simulations of composite delamination. Eng Fract Mech 75(16):4774–4792
37. Qu SS, Yao P, Gong YD et al (2022) Modelling and grinding characteristics of unidirectional C-SiCs. Ceram Int 48(6):8314–8324

**Publisher's Note** Springer Nature remains neutral with regard to jurisdictional claims in published maps and institutional affiliations.

Springer Nature or its licensor (e.g. a society or other partner) holds exclusive rights to this article under a publishing agreement with the author(s) or other rightsholder(s); author self-archiving of the accepted manuscript version of this article is solely governed by the terms of such publishing agreement and applicable law.